Simulations of Quantum Scattering on a Double Barrier Using Complex Absorbing Potentials

Bendik Steinsvåg Dalen

June 4, 2023

Abstract

Numerical simulations of quantum phenomena are often quite computationally expensive due to the large number of grid points needed to ensure accuracy, and to avoid boundary issues. We have tested if complex absorbing potentials can help reduce this cost, while still ensuring accuracy. We found that they are quite capable of doing so, when we look at the transmission probability and momentum distribution.

The specific phenomenon we looked at was that of a particle colliding with a single and double potential barrier. Here we wanted to test their capacity to be used as velocity filters. We found that a single barrier can work fine to filter out low velocities, while a double barrier can be used to filter for a specific range of velocities, given certain conditions.

1 Introduction

A classic experiment within quantum mechanics involves having a particle collide with a potential barrier, and observing the subsequent scattering. Analytical modelling of this set up reveals that part of the wave function will be reflected, while the rest will transmit through the barrier. The transmission happens even when the momentum of the particle is smaller than that which a classical particle would need to go over the barrier. This phenomenon is often known as quantum tunneling, since the quantum particle can effectively pass straight through the barrier. The amount of the wave function which is transmitted increases non-linearly with the velocity of the particle [6].

If we repeat the same experiment, but use two subsequent potential barriers instead, we can observe an even stranger phenomenon. Now the likelihood of transmission will spike or dip at certain velocities. This means that the chance of transmission does not always increase with velocity, which could be caused by the particle interfering with itself [6]. We want to study this phenomenon numerically, and explore how resonances in the wave function affect scattering and tunneling. We also want to explore if this can be used to create a sort of momentum filter for incoming particles.

Numerical simulations of scattering experiments are often quite computationally expensive. This is because a large numerical grid is needed to avoid boundary issues, such as nonphysical reflections or the wave function wrapping around. Much of the wave function on the grid will also be zero, or close to zero, as the wave function is usually only present in parts of the area. In addition, the simulations involves many matrix multiplications, which scale poorly as the number of grid points increases.

One technique which can reduce the computational expense are so called complex absorbing potentials (CAPs) [2]. Here the wave function is absorbed when it is close to the end points of the grid, which can often entirely remove the chance of artificial reflections. This allows us to reduce the size of the numerical grid greatly. It has also been shown that CAPs can be used to extract physical information from the system [5].

One problem with CAPs is that the Hamiltonian of the wave function will no longer be Hermitian, which means we can not use the wave function directly to find physical information about the system. Instead we will need to use techniques such as those detailed in Selstø 2022 [5] or Tao 2012 [7].

Throughout this paper we use atomic units (a.u.), where $\hbar = e = m_e = 1$. All code used can also be found on GitHub: https://github.com/bendkok/PENG9570/tree/main/exercises

2 Theory and Method

Most of this section is based upon Selstø (2023)[6].

The time dependent Schrödinger equation (TDSE) can be written as

$$i\frac{\partial}{\partial t}\Psi(x;t) = \hat{H}\Psi(x;t), \tag{1}$$

where Ψ is the wave function and

$$\hat{H} = -\frac{1}{2}\frac{d^2}{dx^2} + V(x) = \hat{T} + V(x) \tag{2}$$

is the Hamiltonian, where $V(x)$ is the potential energy and $\hat{T}$ is the kinetic energy. For a single potential barrier we set

$$V_s(x) = \frac{V_0}{e^{s(|x|-w/2)}+1}, \tag{3}$$

which is a continuous approximation to a square potential. For a double potential barrier we set

$$V_d(x) = V_s(x-d) + V_s(x+d) = \frac{V_0}{e^{s(|x-d|-w/2)}+1} + \frac{V_0}{e^{s(|x+d|-w/2)}+1}. \tag{4}$$

For the initial wave function we used a Gaussian distribution,

$$\Psi(x, t=0) = \sqrt{\frac{\sqrt{2}\sigma_p}{\sqrt{\pi}\left(1-2i\sigma_p^2\tau\right)}} \exp\left[-\frac{\sigma_p^2\left(x-x_0\right)^2}{1-2i\sigma_p^2\tau} + ip_0x\right], \tag{5}$$

where p_0 is the mean initial velocity of the wave, x_0 is the mean starting position, σ_p is the width of the momentum distribution and τ is a time offset.

TDSE is typically a PDE, as it depends both on time and the position of any relevant particles. However, it can be represented numerically as an ODE by using several approximations. In this section we will detail how this can be done in the scenario where a particle is scattering against a single or double barrier. We will first present a more typical approach, then we will discuss how this can be modified to include complex absorbing potentials.

2.a Discretising the Wave Function and Hamiltonian

The analytical wave function is a continuous function in an infinitely large spacial domain. This cannot be represented on computers, as they only have finite memory and processing power. Instead, we approximate the spatial grid by separating it into discrete units, separated by a fixed distance Δx.

Further, we set some cutoff points for the grid. For the scattering example, it makes the most sense to set these an equal distance from the potential barriers. The assumption here is that the wave function will not have time to reach the cutoff points, thus we do not need to simulate the area further outside.

The wave function is thus approximated by a complex column vector

$$\Psi(x;t) \to \Psi(t) = \begin{pmatrix} \Psi\left(x_0;t\right) \\ \Psi\left(x_1;t\right) \\ \vdots \\ \Psi\left(x_n;t\right) \end{pmatrix}, \tag{6}$$

of length $n+1$. When using such a numerical approximation we want the simulated area and the number of grid points to be as small as possible. However, if the cutoff points are too close we may induce boundary issues. Similarly, if the number of grid points is too small we will get an inaccurate simulation. Thus, balancing these values is an important step when tuning a simulation.

We also need to represent the Hamiltonian in this discretised domain. This is relatively straightforward, since $\hat{H}$ is time independent. Firstly, the potential can be represented as a diagonal matrix,

$$V(x) \to V = \begin{pmatrix} V\left(x_0\right) & 0 & 0 & \\ 0 & V\left(x_1\right) & 0 & \cdots \\ 0 & 0 & V\left(x_2\right) & \\ & \vdots & & \ddots \end{pmatrix}. \tag{7}$$

Discretising the kinetic energy is slightly harder, as it contains a double derivative. Many methods exist to achieve this, e.g. finite difference schemes. Our approach will be to use the Fourier transform to approximate the derivative. After taking the Fourier transform of Ψ, its derivative can easily be found by multiplying with ik, or $-k^2$ for the double derivative. Afterwards, the inverse Fourier transform is used to transform back to the x-transform. This gives

$$\hat{T}\Psi = -\frac{1}{2}\mathscr{F}^{-1}\left\{(ik)^2\mathscr{F}\{\Psi\}\right\} = \frac{1}{2}\mathscr{F}^{-1}\left\{k^2\mathscr{F}\{\Psi\}\right\}. \tag{8}$$

Whit these approximations equation eq. 1 is recast to

$$i\frac{\partial}{\partial t}\Psi(x;t) = \hat{H}\Psi(x;t) \quad \longrightarrow \quad i\frac{\partial}{\partial t}\Psi(t) = \frac{1}{2}\mathscr{F}^{-1}\left\{k^2\mathscr{F}\{\Psi(t)\}\right\} + V\Psi(t). \tag{9}$$

This is a vector ODE, as it only depends on the time t. We now need a strategy to solve this ODE with regard to time.

2.b Numerical Time Propagation

To propagate through time we used the Magnus propagator,

$$\Psi(x;t) = \exp\left[-i\hat{H}t\right]\Psi(x;t=0). \tag{10}$$

Since the Hamiltonian is time independent and Hermitian, the Magnus propagator allow us to jump straight from the initial time to the end time. Other methods, such as the Crank-Nicolson propagator, would instead need to discretise the time domain, and then propagate through small time steps. The same is true for non-Hermitian and/or time dependent Hamiltonians.

If we insert eq. 10 into eq. 9 we get

$$\Psi(t) = \exp\left[-i\hat{H}t\right]\Psi(0) = \exp\left[-i\left(\frac{1}{2}\mathscr{F}^{-1}\left\{k^2\mathscr{F}\{\mathbb{1}\}\right\} + V\right)t\right]\Psi(0). \tag{11}$$

We can replace Ψ inside the Fourier transform with the identity matrix, since we are using linear matrix transforms.

2.c Assessing Results

After running a simulation to the stopping time, we are mainly interested in two properties of the ave function; the transmission and reflection probability ratio, and the momentum probability distribution.

The transmission is the amount of the wave function which has passed through the potential barrier. Its probability can be found with

$$T = \int_0^\infty |\Psi(x)|^2\, dx. \tag{12}$$

The reflection probability can be found similarly

$$R = \int_{-\infty}^0 |\Psi(x)|^2\, dx. \tag{13}$$

These two values should add up to one, which is a good test for our simulation. In terms of numerical implementation, we replace ∞ with the limit of the grid,

$$T = \int_{x_0}^{x_{max}} |\Psi(x)|^2\, dx, \quad R = \int_{x_{min}}^{x_0} |\Psi(x)|^2\, dx. \tag{14}$$

When using a double barrier we can instead use

$$T = \int_d^\infty |\Psi(x)|^2\, dx, \quad R = \int_{-\infty}^{-d} |\Psi(x)|^2\, dx, \tag{15}$$

where d is the distance from the origin to the barriers. This allows us to keep track of amount of the wave function which is trapped between the two barriers, $P_{trapped} = \int_{-d}^{d} |\Psi(x)|^2\, dx$. For $t \to \infty$, all of the wave function will eventually dissipate out, meaning $P_{trapped} \to 0$. We can use this to check that the simulation time is large enough.

The momentum probability distribution tells us how large we can expect the momentum of the simulated particle to be, at any point in time. It is given by

$$\frac{\partial P}{\partial p}(t) = \frac{1}{2\pi}\left|\mathscr{F}\left(\Psi(x;t)\right)\right|^2. \tag{16}$$

After the collision with the potential barrier, we can also split $\frac{\partial P}{\partial p}$ into the momentum for the transmitted and the reflected wave function. This is because a particle which is transmitted will be moving towards the right, and thus have positive $\frac{\partial P}{\partial p}$. The opposite is true for the reflection. This is all assuming the initial wave function starts on the left of the barrier, and moves towards the right (positive x-direction).

2.d Complex Absorbing Potentials

The above details the more typical approach to numerically solving the TDSE. This has the disadvantage that it requires a relatively large grid area. This is because part of the wave function can spread out quite far while a different part is still interacting with the barrier. Since this method needs to simulate the entire wave function, we need a large grid area to ensure the wave function has enough space so that the collision can be completed, but still avoid boundary issues. This subsection will detail how the required grid area can be reduced, by modifying the given method to include so called complex absorbing potentials (CAPs).

CAPs are artificial potentials that are placed at the bounds of the spacial grid. They reduce the value of any part of the wave function that overlaps with them, effectively absorbing it [2]. This is done by replacing the Hamiltonian with

$$H_{\text{eff}} = H - i\Gamma, \tag{17}$$

where H is the old Hamiltonian, and Γ is Hermitian and positive semi-definite. Γ can be chosen to be either local and non-local, however it should only affect the wave function in the area near the boundary.

Of note is that H_{eff} is non-Hermitian. This means we can no longer go directly from $t = 0$ to the end time when uaing the Magnus propagator, eq. 10. Instead we need to discretise the time domain, and iterate over each timestep, with

$$\Psi(t + \Delta t) \approx \exp\left[-i\hat{H}\Delta t\right] \Psi(t). \tag{18}$$

Δt is the change in t for each step. The goal is that the computational gain from reducing the spacial grid is greater than the cost of having to call eq. 18 several times.

Another consequence of using CAPs is that the norm of Ψ will be reduced as the wave function is absorbed near the boundaries. This is not an large issue for the problem we are looking at here. When the norm hits ~ 0, the entire wave function will have been absorbed. Afterwards there will be no significant change in the system, and it serves as a good stopping criteria.

The specific Γ function we used is

$$\Gamma(x) = \begin{cases} \gamma_0(x - R)^2, & |x| > R \\ 0, & \text{otherwise} \end{cases}, \tag{19}$$

which is a local function. Here γ_0 and R are constants which need to be tuned. R can also be expressed as a ratio of x_{max}, i.e. $R = rx_{max}$ with $r \in (0, 1]$.

2.d.i Finding T, R and $\frac{\partial P}{\partial p}$ When Using CAPs

When employing CAPs we cannot use eq. 14 to find T and R, nor eq. 16 to find $\frac{\partial P}{\partial p}$. This is because the norm of Ψ is reduced as the wave function is absorbed, meaning some data is lost each time step. For example, if we used eq. 14 after the norm hits 0 we would get that nothing had been transmitted and nothing had been reflected. These values instead have to be calculated on the fly.

To find the transmission and reflection probabilities we can instead use

$$T = \int_0^\infty dt \Gamma_r(x) \left|\Psi(x)\right|^2, \quad R = \int_0^\infty dt \Gamma_l(x) \left|\Psi(x)\right|^2, \tag{20}$$

where Γ_r and Γ_l are the right and left CAPs respectively. We can take the time derivative of, e.g., T,

$$\frac{dT}{dt} = 2\int_{-\infty}^\infty \Gamma_r(x) \left|\Psi(x)\right|^2 dx, \tag{21}$$

and effectively get a new ODE we can approximate using the same time domain as earlier:

$$T(t + \Delta t) \approx T(t) + 2\Delta t \int_{-\infty}^\infty \Gamma_r(x) \left|\Psi(x)\right|^2 dx. \tag{22}$$

And equivalent for R. This can be calculated alongside the regular simulation.

From Selstø (2022)[5], we get that the momentum distribution can be calculated using

$$\frac{\partial P}{\partial p} = 2\,\text{Re}\int_0^\infty dt \left[\mathscr{F}\left\{\Psi(t)\right\}(p)\right]^* \mathscr{F}\left\{\Gamma(x)\Psi(t)\right\}(p). \tag{23}$$

This can be discretised similarly to eq. 22, giving

$$\frac{\partial P}{\partial p}(t + \Delta t) = \frac{\partial P}{\partial p}(t) + 2\,\text{Re}\left(\left[\mathscr{F}\left\{\Psi(t)\right\}(p)\right]^* \mathscr{F}\left\{\Gamma(x)\Psi(t)\right\}(p)\right). \tag{24}$$

This also can be calculated alongside the regular simulation.

Further, we can see that to get correct results, both eq. 22 and eq. 24 need the simulation time to be long enough so that the entire wave function is absorbed. This is thus no longer just a convenient end point, but also a requirement.

3 Results

3.a Plots of $|\Psi|^2$

In figure 1 and 2 are plots of $|\Psi|^2$ at various points in the simulation. We can see quite good agreement between the two methods. For the CAP the wave function is also nicely absorbed at the boundaries, with no apparent boundary issues.

Movies of the animations can also be found on the GitHub.

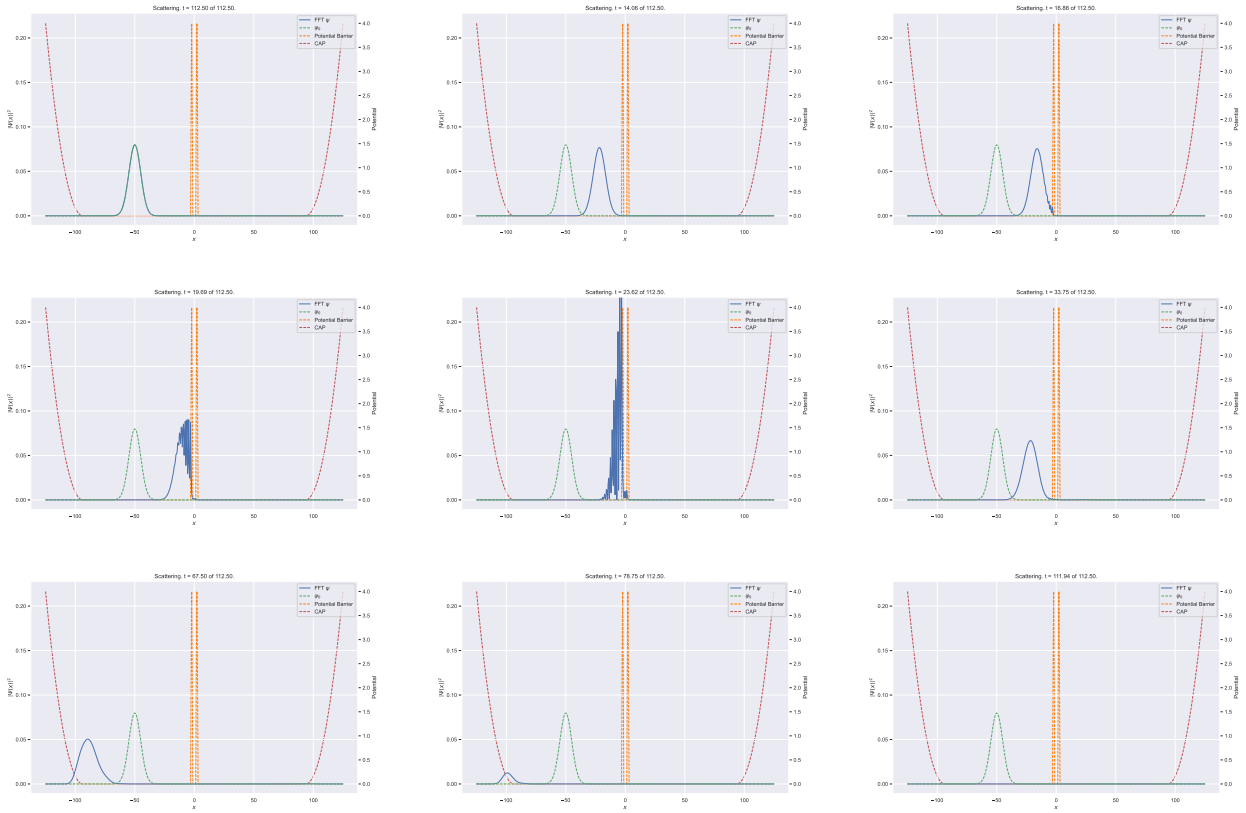

Figure 1: Plots of $|\Psi|^2$ at various points in the simulation, using CAP, and double barrier. With parameters $V_0 = 4, x_0 = -50$ and $p_0 = 2$. The rest are the same as in table 1.

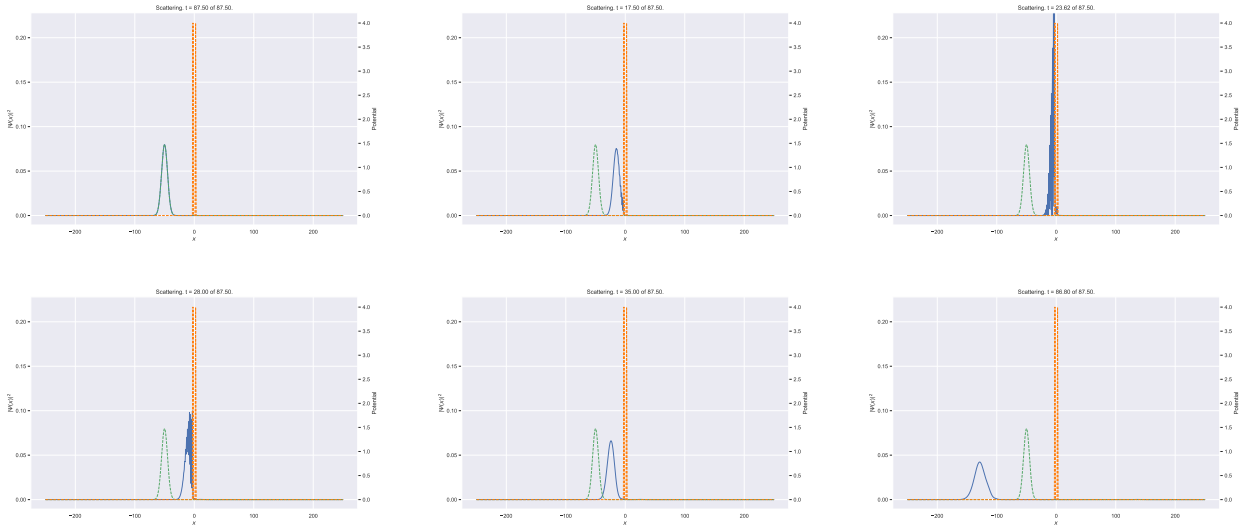

Figure 2: Plots of $|\Psi|^2$ at various points in the simulation, not using CAP, and double barrier. With parameters $V_0 = 4, x_0 = -50$ and $p_0 = 2$. The rest are the same as in table 1.

3.b Comparing Transmission Probability

We first wanted to test the accuracy of the CAP method. This was done by comparing the result from the method without CAP, with the result with CAP, for two different strengths of γ_0 in eq. 19, and two different values of V_0. Both with a single and a double barrier. We ran the simulation for 150 different values of the initial momentum, $p_0 \in [0.4, 6]$ in eq. 5 for each of the scenarios, and compared the resulting transmission probability. The result can be seen in figure 3.

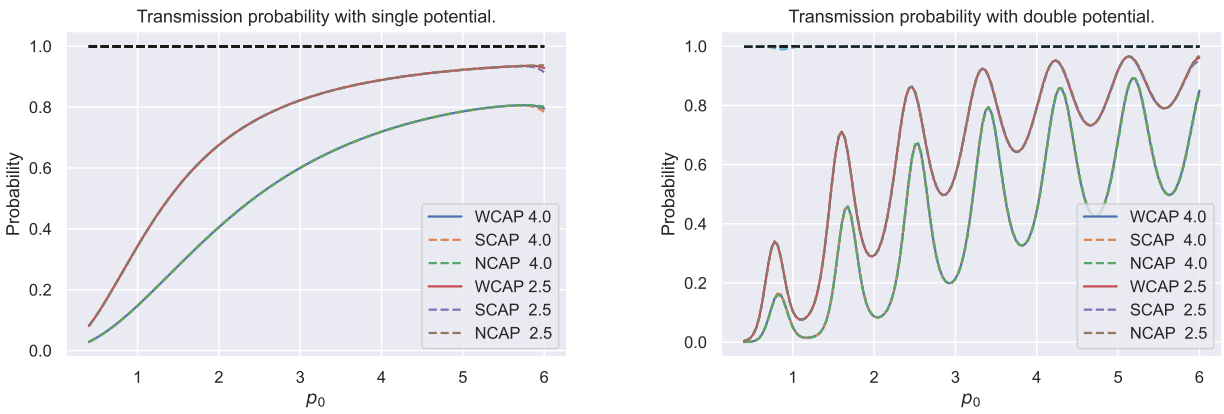

Figure 3: Plots comparing results of transmission probabilities for weak CAP (WCAP), strong CAP (SCAP), and no CAP (NCAP). Also comparing results with $V_0 = 4$ and $V_0 = 2.5$. The CAP simulations were run until all of the wave function had been absorbed. The simulation time without CAP was set to be inversely proportional to p_0. The striped black and cyan lines represents $T + R$, see the text for further details. See table 1 for parameters. Left: Single potential barrier, eq. 3. Right: Double potential barrier, eq. 4.

The agreement is very good, with only a slight difference for the highest values of p_0. This holds true for both the single and the double potential barrier, and with different values of V_0. From this we can conclude that the CAP method is both consistent and accurate with the given numerical parameters, but that we might need to tweak them a bit for if we are working with particularly high velocities.

We also checked that $T + R = 1$ for all the simulations. This is represented by the striped black lines in figure 3, most of which are overlapping. We can see that the equality always held true, except for the no CAP method with $V_0 = 4$. Here there was a slight dip around $p_0 \sim 0.9$, which is represented by the striped cyan line. This indicates that the simulation time was slightly too short, meaning some of the wave function didn't have time to dissipate out from the barrier. However, this does not appear to have a significant effect on the result.

The common parameters used for figure 3 can be found in table 1. Of note is that the no CAP method needed at least twice as many grid points as the method with CAP. The overall runtime for all the 150 simulations was always at least twice as long for the standard approach, showing a clear improvement. However, a comprehensive study of the runtime, and how it scales with different parameters, was not conducted. The CAP approach used a stopping criterion, instead of a fixed simulation time. We noticed that its runtime could vary allot depending on initial velocity. Thus it may be that for certain p_0 the standard approach is faster. However, the CAP method is likely to be faster most of the time.

3.c Comparing Momentum Distribution

For the momentum probability distribution, we first tested that standard and CAP implementations gave the same answer. This is not as straightforward as with transmission, since each p_0 value returns a distribution in p, as opposed to one number. In addition, the difference in grid size means we cannot simply subtract one of the outputs from the other. The best solution we found was to find which grid point of the no CAP output was closest to each CAP point, then find the difference in $\frac{\partial P}{\partial p}$ there. This difference is not exact, but will be close. The result can be seen in figure 4.

For the single barrier we can see a slight difference, particularly for the lowest p_0 and the transmitted wave functions with the highest p_0. Overall it is quite close though. For the double barrier there are some slight differences for low p_0, but overall it is also quite close. We also tried plotting the two results on top of each other, which showed that they have the same general shape. With this we concluded that the results are close enough that we can use CAP without worry.

Next, we studied what shape the momentum distribution would take. In figure 5 we have plotted the resulting $\frac{\partial P}{\partial p}$ for both single and double potential barrier, with two different values of V_0.

For the single potential, we can see that mean p in creases linearly with the input p_0, while the distribution stays mostly the same. For the double barrier, we see the same shape, but with some periodic variation in the

Table 1: The common parameters used in figure 3. Some of the names are explained in the text. The subscript clarifies whether it is for the standard approach (reg) or using CAPs (CAP) when relevant. L is the size of the grid and N is the number of grid points. t_{reg} is the end time for the standard approach. The CAP approach used a stopping criterion of $\sum_n |\Psi(x_n)|^2 \Delta x < 10^{-6}$, instead of a fixed end time. Hence why it only has a Δt.

Parameter	Value
w	0.5
d	2
s	25
x_0	-30
σ_p	0.1
τ	0
L_{CAP}	250
N_{CAP}	512
r	0.75
γ_0	$0.006 \cdot \lvert p_0 \rvert$ or $0.012 \cdot \lvert p_0 \rvert$
Δt_{CAP}	$200 \cdot \left(\frac{L}{4} + \lvert x_0 \rvert\right) / \lvert p_0 s \rvert$
L_{reg}	500
N_{reg}	1024
t_{reg}	$(\frac{L}{4} - \lvert x_0 \rvert)/\lvert p_0 \rvert$

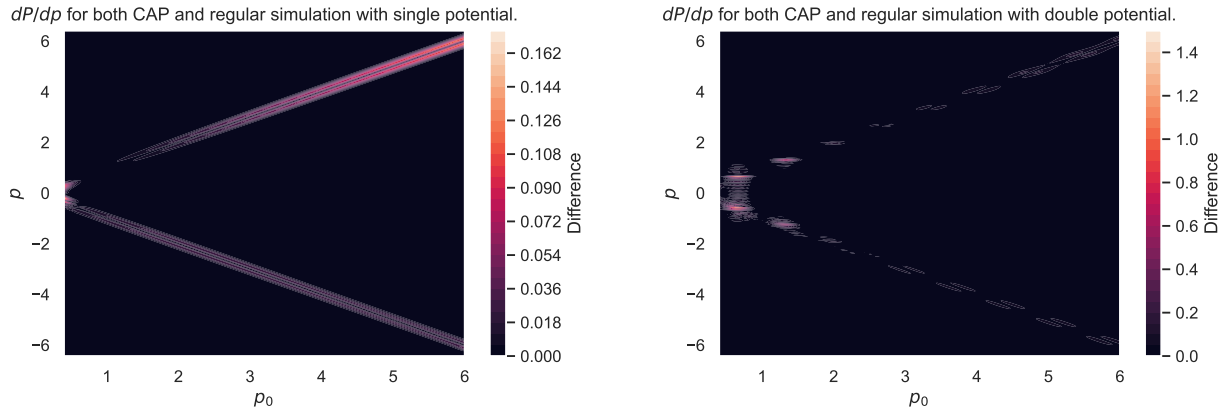

Figure 4: Absolute difference in momentum probability distribution between CAP and no CAP, with $V_0 = 4$. Left: Single potential barrier. Right: Double potential barrier.

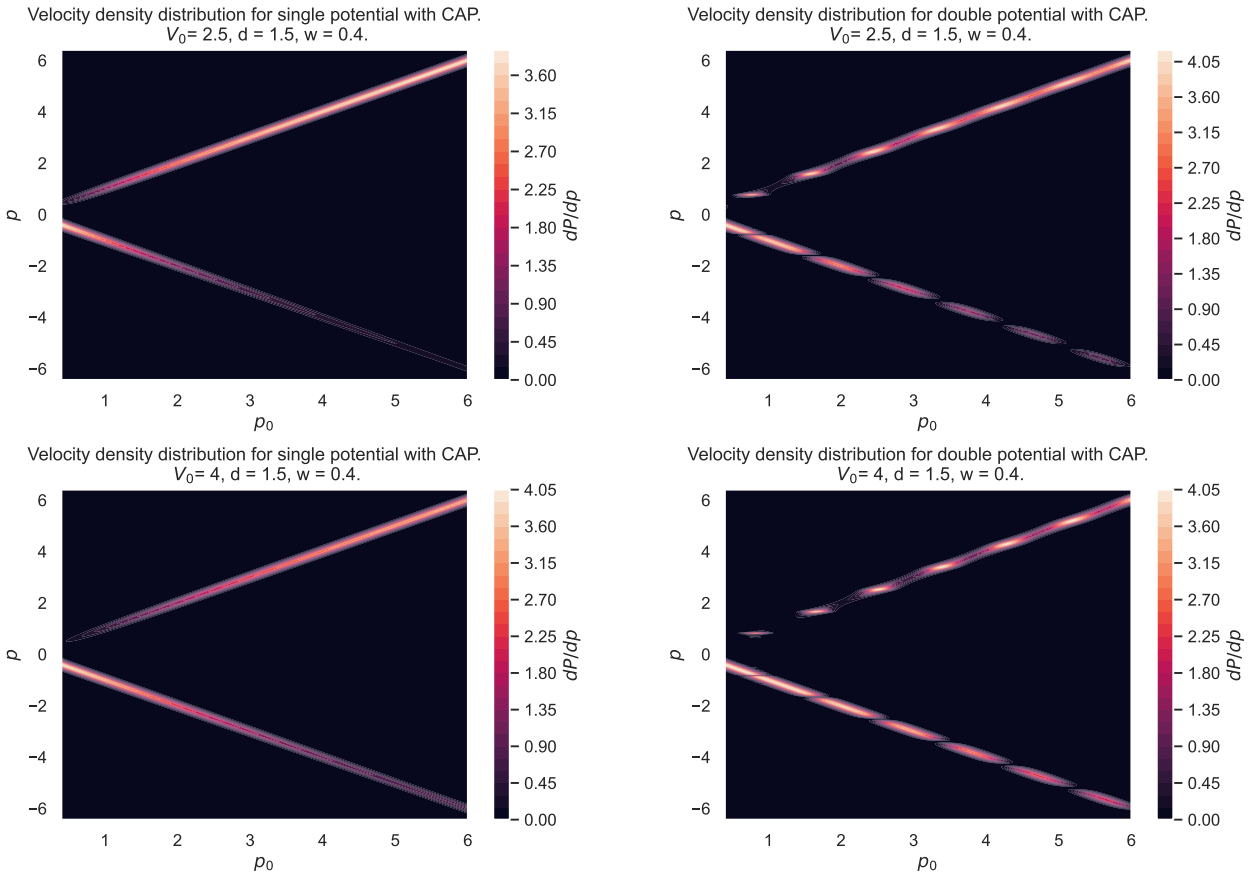

Figure 5: Momentum probability distribution with $V_0 = 2.5$ and 4, using CAP. Positive p is from the transmitted wave, while negative is from the reflected.

intensity. These likely correspond to the resonances of the waves. Also of note is that the two potentials gives mostly the same shape, but with some difference in intensity. For the lowest resonance of the double potential it appears as if the transmitted output is horizontal. This would mean that several values of p_0 gives the same mean p value, though the distribution may vary slightly. This last observation could be useful for a momentum barrier.

3.d Use as a Momentum Filter

Finally, we studied how well this the double potential barrier could function as a momentum filter. We ran the same simulation as earlier, but now with much stronger potential barriers, $V_0 = 8$ and 10. See figure 6.

Now we see that the transmitted output is horizontal for all the resonances. However, resulting mean p is different between each of them. In addition, the intensity of the transmitted $\frac{\partial P}{\partial p}$ are quite low.

From all of this we can conclude that if we knew that all incoming particles were within a certain band of velocities, we could filter them to only get particles within a small distribution around a mean momentum. However, such a filter would also block many of the particles within this distribution. There would also be a small chance that some particles outside the desired distribution would filter through. Though this is almost unavoidable when dealing with quantum particles.

On the other hand, if the only desire was for the filtered particles to be above a certain level of momentum, a single potential barrier could work quite well.

4 Conclusions

In this paper we have explored the use of CAPs to simulate a quantum phenomena. Specifically that of a particle colliding with a single or double potential barrier.

We have seen that an implementation with CAPs is fully capable of producing equivalent results with the more standard simulation approach, but with less computational cost and memory requirements. This is in terms of the shape of the wave function, the transmission probability, and the momentum distribution.

We have also seen that the double potential barrier can be used as a momentum filter. Though this is only if the velocity of the incoming particles fall within a certain range. In addition, many particles that does have the

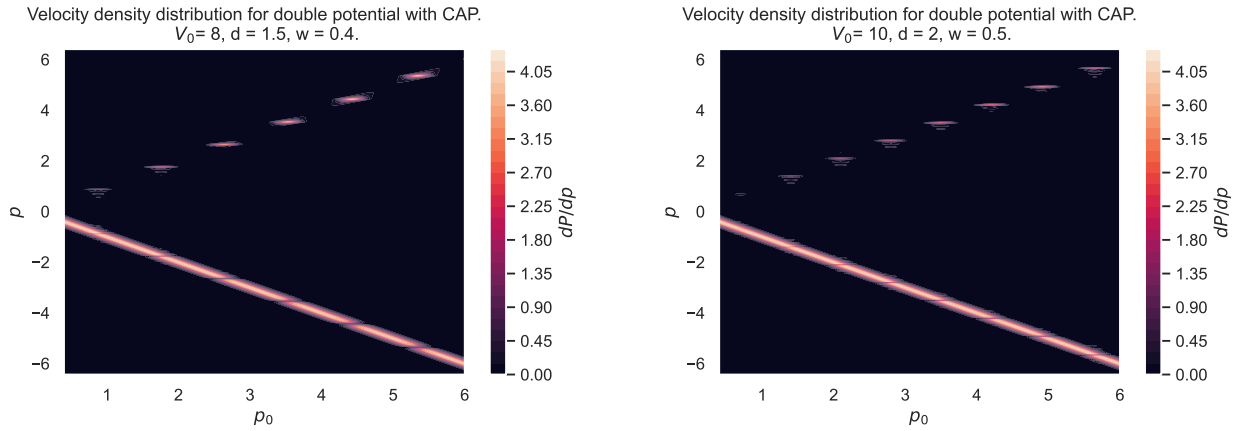

Figure 6: Momentum probability distribution with CAP, a double potential barrier. Left: $V_0 = 8$. Right: $V_0 = 10$.

desired momentum may still be reflected by such a filter. On the other hand, a single potential barrier could work quite as a high pass filter.

4.a On Using the Model for Optimisation

Finally, we wanted to conclude with an outlook on using this model for optimisation. For example, if we wanted to filter incoming particles for a specific mean momentum and distribution, could we use the presented CAP model to optimise the physical parameters of the barrier, V_0, d and w?

Firstly, are the problems we outlined earlier; the incoming particles need to be within a specific range, and many of the ones with appropriate levels of momentum would be filtered out. However, these does not appear to be insurmountable problems. We can thus assume that this is accounted for. Alternatively, we could want to optimise a single barrier to have a certain threshold for incoming particles.

Another potential problem is that the model is potentially not accurate enough to real life conditions, and thus the result cannot be used. A real life implementation would be needed to test this.

An obvious candidate for optimisation would be to use a form of gradient descent. We would need some optimisation criterion and some form of input data. For the former we could use mean value and the standard deviation of the resulting $\frac{\partial P}{\partial p}$ and compare it to the desired ones. Alternatively we could use the whole array output, and compare it to a Gaussian distribution made using the target mean and deviation values. In terms of input data, the best option would likely be to use some random variety in p_0, σ_p, x_0 and maybe even τ.

Further, we do not have access to an analytical derivative, so we would need to approximate it, for example using trapezoidal integration. This would require us to run a full simulation twice for each parameter, six times in our case, repeat for each data point, and repeat again for each epoch. All this would likely require a lot of computation time. With modern supercomputers this might be overcome, though it could also be the case that result is not worth all the computational cost. Further testing would be needed here.

Optimisation methods with a specific application for simulations also exists. E.g. response surface methodology [4], derivative-free optimization [1] or heuristic methods [3]. These might work better than gradient descent.

References

[1] A. R. Conn, K. Scheinberg, and L. N. Vicente. *Introduction to derivative-free optimization.* SIAM, 2009.

[2] R. Kosloff and D. Kosloff. Absorbing boundaries for wave propagation problems. *Journal of Computational Physics*, 63(2):363–376, 1986.

[3] J. Pearl. *Heuristics: intelligent search strategies for computer problem solving.* Addison-Wesley Longman Publishing Co., Inc., 1984.

[4] M. Rahimi Mazrae Shahi, E. Fallah Mehdipour, and M. Amiri. Optimization using simulation and response surface methodology with an application on subway train scheduling. *International Transactions in Operational Research*, 23(4):797–811, 2016.

[5] S. Selstø. Absorbers as detectors for unbound quantum systems. *Physical Review A*, 106(4):042213, 2022.

[6] S. Selstø. Playing around with the schrödinger equation. *Shared privatley as part of course syllabus*, 2023.

[7] L. Tao and A. Scrinzi. Photo-electron momentum spectra from minimal volumes: the time-dependent surface flux method. *New Journal of Physics*, 14(1):013021, 2012.